Front. Electr. Electron. Eng. China 2008, 3(3): 358–363
DOI 10.1007/s11460-008-0052-0

RESEARCH ARTICLE

Junhong MAO, Junhang LUO, Qiang JIANG, Youbai XIE

Design of magnet arrays for permanent magnetic linear motor

Abstract An iron-less single side permanent magnetic linear motor structure is presented, and two-dimensional analytical formulae for its magnetic field are deduced to design the types of magnetic arrays, the thickness of permanent magnet, and the duty ratio of magnet arrays, etc. With certain design parameters, conventional arrays are used instead of a piecewise Halbach arrays, and the machining and assembling of the motor are greatly simplified. Calculation results coincide with that of ANSYS. The analytical formulae can be used in designing cored linear motors by modifying boundary conditions. A linear motor driven bench with a single degree of freedom is realized, where the travel reaches 27 mm, the mass of the moving parts is 1.4 kg, and the maximum acceleration is 11.5 m/s^2.

Keywords linear motor, permanent magnet array, parameter design

1 Introduction

In a translational motion system driven by a linear motor, any mechanical translation that is a must when the system is driven by a rotational motor is no longer used. A linear motor realizes directly driving from a motor to worktable. Therefore, the mechanical structure of a translational motion system is simplified with fewer non-linear parts, and better dynamic performance can be expected. Linear motors and direct driving technology are very important for high precision, high acceleration and high reliability motion control [1].

Translated from *Journal of Xi'an Jiaotong University*, 2007, 41(3): 353–357 [译自: 西安交通大学学报]

Junhong MAO (✉), Junhang LUO, Qiang JIANG, Youbai XIE
School of Mechanical Engineering, Xi'an Jiaotong University, Xi'an 710049, China
E-mail: jhmao@mail.xjtu.edu.cn

Qiang JIANG
School of Electrical Engineering, Xi'an Jiaotong University, Xi'an 710049, China

Similar to rotational motors, linear motors fall into several categories, among which the servo performance of a permanent magnet synchronous linear motor is the best [2,3]. Figure 1 shows a one-degree-of-freedom (1-DOF) directly driving translational motion system and the structure of the linear motor designed in this paper. The linear motor is an iron-less single side permanent magnet synchronous linear motor. In this paper, a two-dimensional vector potential of the air gap of the motor is calculated from the Poisson equation and an analytical solution of the magnetic flux density is obtained. The relationship between design parameters of permanent magnetic arrays and the magnetic field of the motor is analyzed and discussed. Magnetic fields magnetized by Halbach and conventional arrays with two duty ratios are also given and compared with each other. Conventional arrays with one calculated duty ratio is adopted and realized as shown in Fig. 1. The effect of coil current in the magnetic field is not discussed since there is no iron core and ampere turns are low (ampere turns of one coil are less than 100 A). Thus the armature reaction is so slight that it can be neglected. In Fig. 1(b), the permanent magnetic arrays are conventional arrays, the

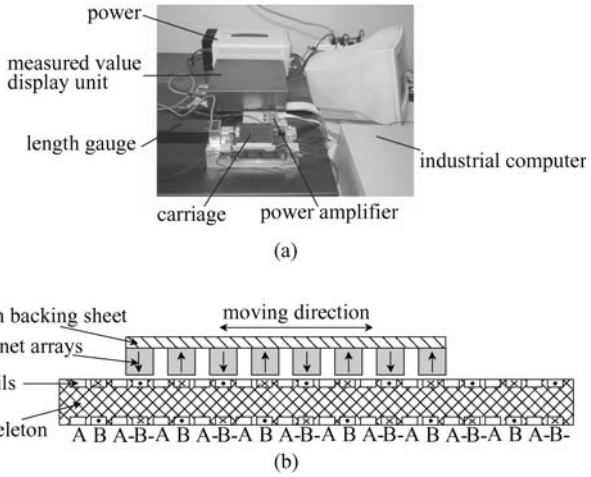

Fig. 1 Translational motion system driven by linear motor and structure of motor. (a) Direct-drive linear displacement system; (b) structure scheme of linear motor

windings are two-phase concentrated coils, and the electrical angle between two neighboring coils is 90°.

The prototype shown in Fig. 1 is featured as follows:

1) There is no iron core, which leads to low inductance and wide closed-loop bandwidth.

2) The winding is designed as the stator and fixed to the frame, and the permanent magnet arrays are attached to the mover, thus no electrical connection is needed between the mover and frame nor is there any thermal deformation caused by copper loss.

3) Single-side form is adopted and the mechanical structure of the motor is simplified.

4) There is no vertical force, thus frictional force of the guide way is decreased.

5) There is no cogging force, therefore thrust ripple is decreased and servo performance is improved.

6) There is no electric brush, which leads to less nonlinearity of friction, high reliability and long life.

7) There is no magnetic saturation and high acceleration can be reached.

2 Analytical analysis of permanent magnetic linear motor field

The permanent magnetization equation for permanent magnet of Nd-Fe-B can be approximated by

$$\boldsymbol{B}=\mu_0\boldsymbol{H}+\mu_0\boldsymbol{M}_{\mathrm{r}}=\mu_0\boldsymbol{H}+\boldsymbol{B}_{\mathrm{r}}, \tag{1}$$

where $\boldsymbol{B}$ is magnetic flux density, T; $\boldsymbol{H}$ is magnetic field intensity, A/m; $\boldsymbol{M}_{\mathrm{r}}$ is remanence magnetization of the permanent magnetic materials, A/m; $\boldsymbol{B}_{\mathrm{r}}$ is remanence vector, T; $\mu_0=4\pi\times10^{-7}$ H/m is the permeability of free space.

In a static electromagnetic field with permanent magnets, Maxwell's equations are

$$\nabla\times\boldsymbol{H}=\boldsymbol{J}, \tag{2}$$

$$\nabla\cdot\boldsymbol{B}=0, \tag{3}$$

where $\boldsymbol{J}$ is free volume current density, A/m^2. The boundary conditions for the contacting surface of different materials can be derived from Eqs. (2) and (3), which are

$$\boldsymbol{n}\times\left(\boldsymbol{H}^{\mathrm{a}}-\boldsymbol{H}^{\mathrm{b}}\right)=\boldsymbol{K}_{\mathrm{f}}, \tag{4}$$

$$\boldsymbol{n}\cdot\left(\boldsymbol{B}^{\mathrm{a}}-\boldsymbol{B}^{\mathrm{b}}\right)=0, \tag{5}$$

where, superscript a and b represent the associated quantities evaluated on opposite sides of a boundary; $\boldsymbol{K}_{\mathrm{f}}$ is a source surface current directed along the boundary, A/m.

Let $\boldsymbol{A}$ be magnetic vector potential. For a static magnetic field, if the Coulomb gauge [4] $\nabla\cdot\boldsymbol{A}=0$ is adopted, then there is

$$\nabla\times\boldsymbol{B}=\nabla\times\nabla\times\boldsymbol{A}=\nabla(\nabla\cdot\boldsymbol{A})-\nabla^2\boldsymbol{A}=-\nabla^2\boldsymbol{A}. \tag{6}$$

Combining Eq. (6) with Eqs. (1) and (2) yields the vector Poisson equation:

$$\nabla^2\boldsymbol{A}=-\mu_0(\boldsymbol{J}_{\mathrm{f}}+\nabla\times\boldsymbol{M}_{\mathrm{r}}). \tag{7}$$

In the above equation, $\boldsymbol{J}_{\mathrm{f}}$ is volume current density, A/m^2. Combining boundary conditions Eqs. (4) and (5), $\boldsymbol{A}$ can be solved from Eq. (7). The magnetic flux density of the field can be obtained by calculating the operation of the curl of vector $\boldsymbol{A}$.

If the magnetization vector of a permanent magnet varies with a sinusoidal function, the magnetization is represented as:

$$\boldsymbol{M}=\boldsymbol{i}_x\boldsymbol{M}_{\mathrm{r}}\sin kx+\boldsymbol{i}_y\boldsymbol{M}_{\mathrm{r}}\cos kx, \tag{8}$$

where $k=2\pi/\lambda$ is the wave number of the magnet arrays; λ is the spatial period of the arrays, m; $\boldsymbol{M}$ is the magnetization vector of the permanent magnet, A/m; and $\boldsymbol{M}_{\mathrm{r}}$ is the amplitude of the magnetization components, A/m. Equation (8) is the ideal magnetization vector of Halbach arrays. Obviously, it is not possible for a magnet to follow Eq. (8). Thus a practical approach for implementing Halbach arrays is assembling blocks of magnets that are each uniformly magnetized in a desired axis [5]. Such arrays are called piecewise Halbach arrays. Arrays with $N=4$ are shown in Fig. 2, where the thickness and width of the permanent magnets are h and d respectively. Build the coordinate system with the positive x direction horizontally pointing to the right as well as positive y direction vertically upwards. In Fig. 2, Region 1 is iron-backing-sheet region (the relative permeability is approximately infinite with iron backing sheet, and is approximately zero without iron backing sheet). Region 2 is permanent-magnet region. Region 3 is the air gap. The magnetization vector of piecewise Halbach arrays is represented by the Fourier series:

$$\boldsymbol{M}=\sum_{\gamma=0}^{\infty}\boldsymbol{M}_{\mathrm{r}}\frac{\sin(n\varepsilon\pi/N)}{n\pi/N}\left[\boldsymbol{i}_x\sin nkx+\boldsymbol{i}_y\cos nkx\right]+\sum_{\gamma=0}^{\infty}\boldsymbol{M}_{\mathrm{r}}\frac{\sin(n'\varepsilon\pi/N)}{n'\pi/N}\left[-\boldsymbol{i}_x\sin n'kx+\boldsymbol{i}_y\cos n'kx\right], \tag{9}$$

where $n=\gamma N+1$ and $n'=(\gamma+1)N-1$ are the order of harmonics; $\varepsilon=Nd/\lambda$ is the duty ratio of permanent magnet

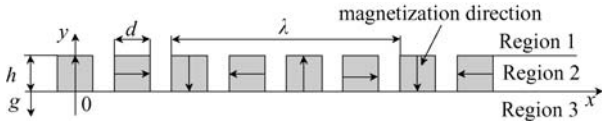

Fig. 2 Schematic diagram of piecewise Halbach arrays ($N=4$)

arrays; d is the width of the permanent magnet, m; λ is the pitch of the arrays. Piecewise Halbach arrays quite equal an superposition of a magnetic field of ideal Halbach arrays $M_{xn}=M_{yn}$ and $M_{xn}=-M_{yn}$, according to Eq. (9).

In two-dimensional cases where the fields lie in the x-y plane with no dependency on z, the vector potential is purely z-directed. Thus $A_x=A_y=0$, and the magnetic flux density is:

$$B_x=\frac{\partial A_z}{\partial y},\quad B_y=-\frac{\partial A_z}{\partial x}, \tag{10}$$

where B_x and B_y are magnetic flux density vector components through the directions of x and y respectively.

Without iron backing sheet, the nth-order magnetic flux density vector of ideal Halbach arrays is:

$$\boldsymbol{M}=\boldsymbol{i}_x M_{xn}\sin nkx+\boldsymbol{i}_y M_{yn}\cos nkx. \tag{11}$$

The vector potential can be expressed by the equations:

$$\begin{cases}\nabla^2 A_{zn1}=-\mu_0\left(J_{f1}+\dfrac{\partial M_{y1}}{\partial x}-\dfrac{\partial M_{x1}}{\partial y}\right)=0,\\ \nabla^2 A_{zn2}=-\mu_0\left(J_{f1}+\dfrac{\partial M_{y1}}{\partial x}-\dfrac{\partial M_{x1}}{\partial y}\right)=\mu_0 nkM_{yn}\sin nkx,\\ \nabla^2 A_{zn3}=-\mu_0\left(J_{f1}+\dfrac{\partial M_{y3}}{\partial x}-\dfrac{\partial M_{x3}}{\partial y}\right)=0\end{cases} \tag{12}$$

with the boundary conditions:

$$\begin{cases}y=0,\ B_{y2}=B_{y3},\ H_{x2}=H_{x3},\\ y=h,\ B_{y1}=B_{y2},\ H_{x1}=H_{x2}.\end{cases} \tag{13}$$

Here subscripts 1, 2 and 3 denote Regions 1, 2 and 3.

A_{zn} can be solved by using separated variable method [6], then according to Eq. (10), the magnetic flux density of the air gap is:

$$\begin{cases}B_{xn3}=-\dfrac{\mu_0}{2}\left(1-\mathrm{e}^{-nkh}\right)\left(M_{yn}+M_{xn}\right)\mathrm{e}^{nky}\sin nkx,\\ B_{yn3}=\dfrac{\mu_0}{2}\left(1-\mathrm{e}^{-nkh}\right)\left(M_{yn}+M_{xn}\right)\mathrm{e}^{nky}\cos nkx.\end{cases} \tag{14}$$

By the superposition principle, without iron backing sheet, magnetic flux density of air gap can be described as:

$$\begin{cases}B_{x3}=-\mu_0\boldsymbol{M}_{\mathrm{r}}\sum\limits_{\gamma=0}^{\infty}\dfrac{\sin(n\varepsilon\pi/N)}{n\pi/N}\left(1-\mathrm{e}^{-nkh}\right)\mathrm{e}^{nky}\sin nkx,\\ B_{y3}=\mu_0\boldsymbol{M}_{\mathrm{r}}\sum\limits_{\gamma=0}^{\infty}\dfrac{\sin(n\varepsilon\pi/N)}{n\pi/N}\left(1-\mathrm{e}^{-nkh}\right)\mathrm{e}^{nky}\cos nkx.\end{cases} \tag{15}$$

According to Eq. (15), the air gap magnetic flux density of the piecewise Halbach arrays without iron backing sheet is the addition of harmonics, whose order is $n=\gamma N+1$. Amplitudes of the nth-order vertical and horizontal Fourier magnetization components are equal, and the phase difference is $\pi/2$. With the increase of n, amplitudes of the harmonics decrease rapidly.

With the boundary conditions:

$$\begin{cases}y=0,\ B_{y2}=B_{y3},\ H_{x2}=H_{x3},\\ y=h,\ B_{y1}=B_{y2},\ H_{x2}=0,\end{cases} \tag{16}$$

we can get the solution to the air gap magnetic flux density of piecewise Halbach arrays with iron backing sheet by solving Eq. (12):

$$\begin{cases}B_{x3}=-\sum\limits_{\gamma=0}^{\infty}\mu_0\boldsymbol{M}_{\mathrm{r}}\dfrac{\sin(n\varepsilon\pi/N)}{n\pi/N}\left(1-\mathrm{e}^{-nkh)}\right)\mathrm{e}^{nky}\sin nkx\\ \qquad -\sum\limits_{\gamma=0}^{\infty}\mu_0\boldsymbol{M}_{\mathrm{r}}\dfrac{\sin(n'\varepsilon\pi/N)}{n'\pi/N}\left(1-\mathrm{e}^{-n'kh}\right)\mathrm{e}^{n'k(y-h)}\sin n'kx,\\ B_{y3}=\sum\limits_{\gamma=0}^{\infty}\mu_0\boldsymbol{M}_{\mathrm{r}}\dfrac{\sin(n\varepsilon\pi/N)}{n\pi/N}\left(1-\mathrm{e}^{-nkh}\right)\mathrm{e}^{nky}\cos nkx\\ \qquad +\sum\limits_{\gamma=0}^{\infty}\mu_0\boldsymbol{M}_{\mathrm{r}}\dfrac{\sin(n'\varepsilon\pi/N)}{n'\pi/N}\left[\left(1-\mathrm{e}^{-n'kh}\right)\mathrm{e}^{n'k(y-h)}\right]\cos n'kx.\end{cases} \tag{17}$$

Compared with Eq. (15), it can be seen that the air-gap magnetic field of piecewise Halbach arrays with iron backing sheet has additional $(n'=(\gamma+1)N-1)$th-order harmonic components compared with that without iron backing sheet.

3 Design parameters of permanent magnet arrays

3.1 Array type

The type of permanent magnet arrays is determined by the parameter N. If $N=2$, the magnetizing direction of the permanent magnets is perpendicular to the air gap and opposite for neighboring permanent magnets, which forms conventional arrays. For conventional arrays without an air backing sheet, Eq. (15) can be written as:

$$B_{y(N=2)}=\sum_{\gamma=0}^{\infty}\mu_0\boldsymbol{M}_{\mathrm{r}}\frac{\sin(n\varepsilon\pi/2)}{n\pi/2}(1-\mathrm{e}^{-nkh})\mathrm{e}^{-nky}\cos nkx,\quad n=2\gamma+1. \tag{18}$$

For conventional arrays with an air backing sheet, Eq. (17) can be written as:

$$B_{y(N=2)}=\sum_{\gamma=0}^{\infty}\mu_0\boldsymbol{M}_{\mathrm{r}}\frac{\sin(n\varepsilon\pi/2)}{n\pi/2}\left(1-\mathrm{e}^{-2nkh}\right)\mathrm{e}^{-nky}\cos nkx,\quad n=2\gamma+1. \tag{19}$$

From the above two equations, it can be seen that the magnetic flux density determined by Eq. (19) equals

to that of Eq. (18) with one-time larger magnet thickness. Meanwhile, an air backing sheet possesses a favorable shielding effect against the magnetic field. Therefore, for conventional permanent magnet arrays, an air backing sheet can improve the performance of motors. In the analysis and calculation below, conventional arrays are always with air backing sheets except otherwise noted.

When $N > 2$, the air gap magnetic flux density of the air-gap magnetic field with and without an air backing sheet is determined by Eqs. (15) and (17) respectively. With the increase of N, the magnetization vector of permanent magnet arrays approaches to ideal Halbach arrays, but the machining and assembly of permanent magnet arrays become more difficult. When $N = 4$, two neighboring magnets are perpendicularly magnetized. Thus the arrays can be realized by magnets with magnetization direction perpendicular to its surface, which makes easier the machining of permanent magnets. In addition, if the permanent magnet has a square cross section, $h = d$, the piecewise Halbach arrays with $N = 4$ can be obtained by using same permanent magnets. Equation (20) describes air-gap magnetic field without an air backing sheet, and Eq. (21) is about the magnetic field with an air backing sheet.

$$B_{y(N=4)} = \sum_{\gamma=0}^{\infty} \mu_0 \boldsymbol{M}_{\mathrm{r}} \frac{\sin(n\varepsilon\pi/4)}{n\pi/4} \left(1 - \mathrm{e}^{-nkh}\right) \mathrm{e}^{-nky} \cos nkx, \quad n = 4\gamma + 1, \tag{20}$$

$$B_{y(N=4)} = \sum_{\gamma=0}^{\infty} \mu_0 \boldsymbol{M}_{\mathrm{r}} \frac{\sin(n\varepsilon\pi/4)}{n\pi/4} \left(1 - \mathrm{e}^{-nkh}\right) \mathrm{e}^{-nky} \cos nkx + \sum_{\gamma=0}^{\infty} \mu_0 \boldsymbol{M}_{\mathrm{r}} \frac{\sin(n'\varepsilon\pi/4)}{n'\pi/4} \left(1 - \mathrm{e}^{-n'kh}\right) \mathrm{e}^{-n'k(y-h)} \cos n'kx, \quad n = 4\gamma + 1,\ n' = 4\gamma + 3. \tag{21}$$

From Eqs. (20) and (21), it can be seen that the employment of an air backing sheet does not affect the fundamental frequency component of the magnetic field. Some additional high-order harmonic components appear when an air backing sheet is used.

3.2 Thickness of permanent magnets

With all high-order harmonics ignored, and zero gap between adjacent permanent magnets assumed, Fig. 3 illustrates the difference between two zero-gap magnetic fields corresponding to conventional arrays in Eq. (20) and Halbach arrays in Eq. (21) respectively. It can be seen from Fig. 3 that when $h/d > 0.8$, the air-gap magnetic flux density of Halbach arrays is larger than that of conventional arrays, and this disparity increases with the thickness of permanent magnet; when $h/d < 0.8$, the air-gap magnetic flux density of conventional arrays is higher than that of Halbach arrays. Particularly, when $h/d = 1$, which means the piece of the permanent magnet with a square cross-section, the two magnetic fields have little difference.

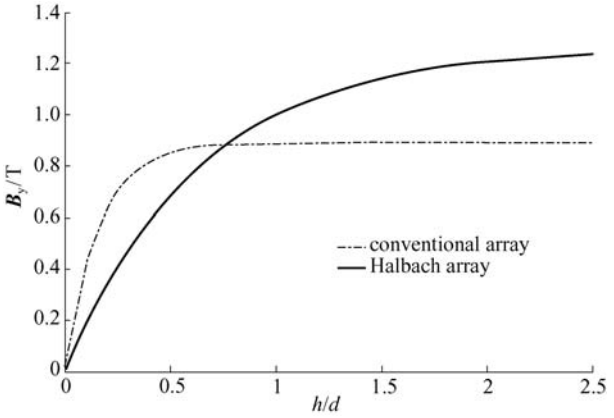

Fig. 3 Change of air-gap magnetic field of conventional and Halbach arrays with h/d

3.3 Duty ratio

In practice, due to installation and support reasons, there is always certain gap, represented by duty ratio ε, between permanent magnets. For conventional arrays and Halbach arrays without an air backing sheet, when $\varepsilon = 1/(1 + 1/N)$, the first higher-order harmonic of magnetic field can be eliminated. Therefore the air-gap magnetic field coordinates sinusoidal better.

Figure 4 shows the y-component of fundamental frequency magnetic flux density of both conventional and Halbach arrays when $N = 4$, $y = -0.5$ mm with the permanent magnet in a square cross-section. As can be seen from Fig. 4, the magnetic flux density of conventional arrays decreases slowly and that of Halbach decreases sharply while ε decreases (the gap between permanent magnets becomes lager). That is, conventional arrays are less sensitive to the change of ε, making it easier for producing, machining and assembly.

4 Design examples of permanent magnet arrays

Parameters of permanent magnet arrays are shown in Table 1. Figures 5 and 6 show the magnetic flux density of Halbach arrays ($N = 4$) and conventional arrays with an iron backing sheet at position $y = -0.5$ mm for different ε respectively. To verify the deduced analytic calculation method, Figs. 5 and 6 give the corresponding calculating results of ANSYS. In the finite element analysis (FEA), plane53 entity unit is used for element mesh division; far-field unit is used to represent external

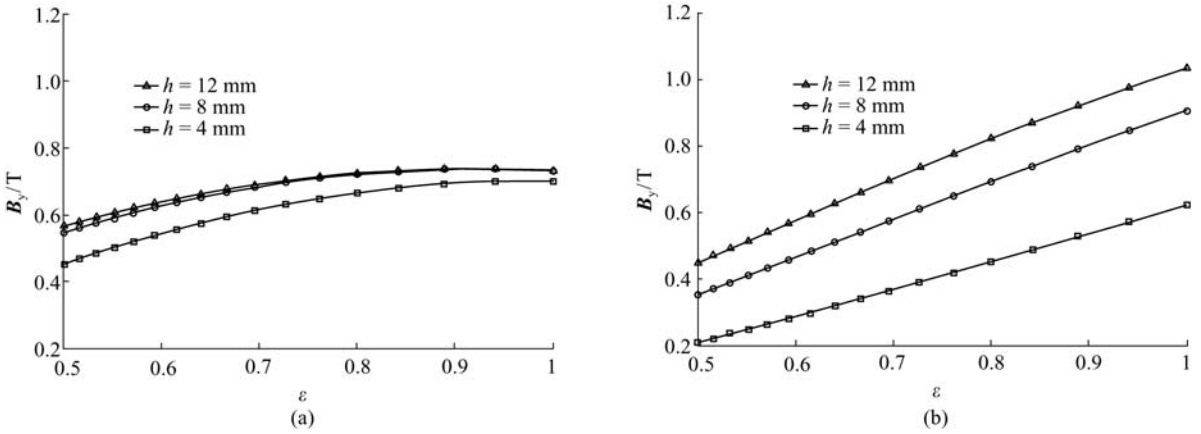

Fig. 4 Changes of amplitude of fundamental frequency magnetic field of conventional and Halbach arrays with ε and h. (a) Conventional arrays; (b) Halbach arrays

conditions of open boundary field model. The value of the relative permeability is 1500 in Region 1 (iron-backing-sheet region).

Table 1 Parameters of permanent magnetic arrays

parameter	value
remanence vector $\boldsymbol{B}_r$/T	1.4
length w/m	0.04
width d/m	0.008
thickness h/m	0.008

The calculated results indicate that the magnetic field of conventional arrays coordinates sinusoidal better than that of Halbach arrays. The advantage is obvious when the gap between permanent magnets becomes large. There is no great difference between the amplitude of the magnetic flux density of conventional and Halbach arrays when ε is 0.62. However, the fundamental frequency component of conventional arrays is larger than that of Halbach arrays. Therefore, there is little cogging force when conventional arrays are used. When ε is 0.89, the amplitude of the magnetic flux density of Halbach arrays are larger than that of conventional arrays. But it is too difficult to construct these magnetic arrays. Based on the above analysis, some parameters are determined, including array type ($N = 2$), cross-section of permanent magnet ($h = d = 8$ mm), and duty ratio $\varepsilon = 0.62$ (spacing 5 mm and array pitch $\lambda = 52$ mm). Figure 7 shows the mover of the linear motor with permanent magnet arrays.

5 Conclusions

In this paper, an iron-less single side permanent magnetic linear motor is designed and two-dimensional analytical formulae for magnet field calculation are given. Magnetization effects of conventional arrays with that of Halbach arrays are compared. The relationship between the magnetized fields and magnet geometric and array parameters are also discussed. The analysis shows that with the linear motor designed in this paper, the same magnetic field could be obtained using conventional arrays instead of Halbach arrays, the machining and assembly of the permanent magnetic linear motor is

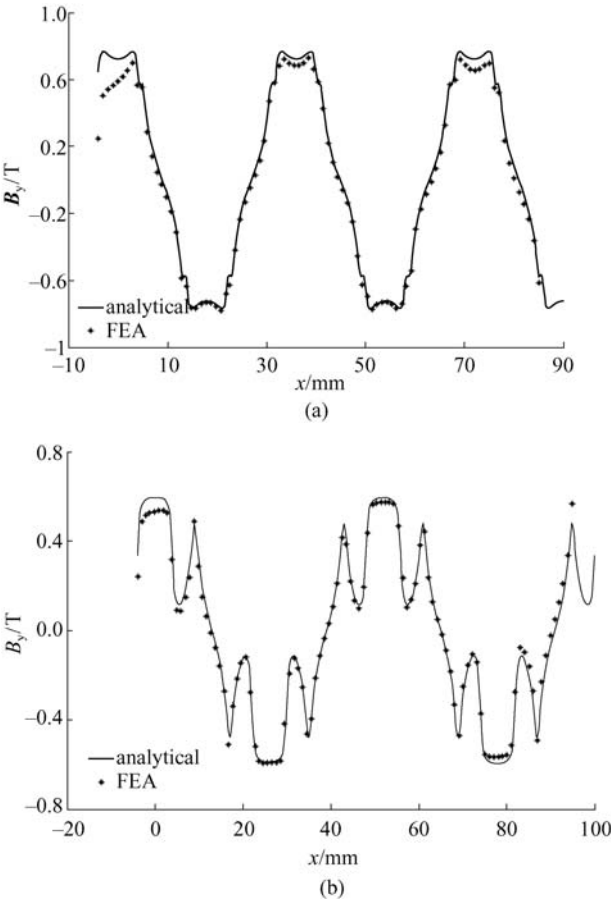

Fig. 5 Air-gap flux density distribution of Halbach arrays. (a) $\varepsilon = 0.89$; (b) $\varepsilon = 0.62$

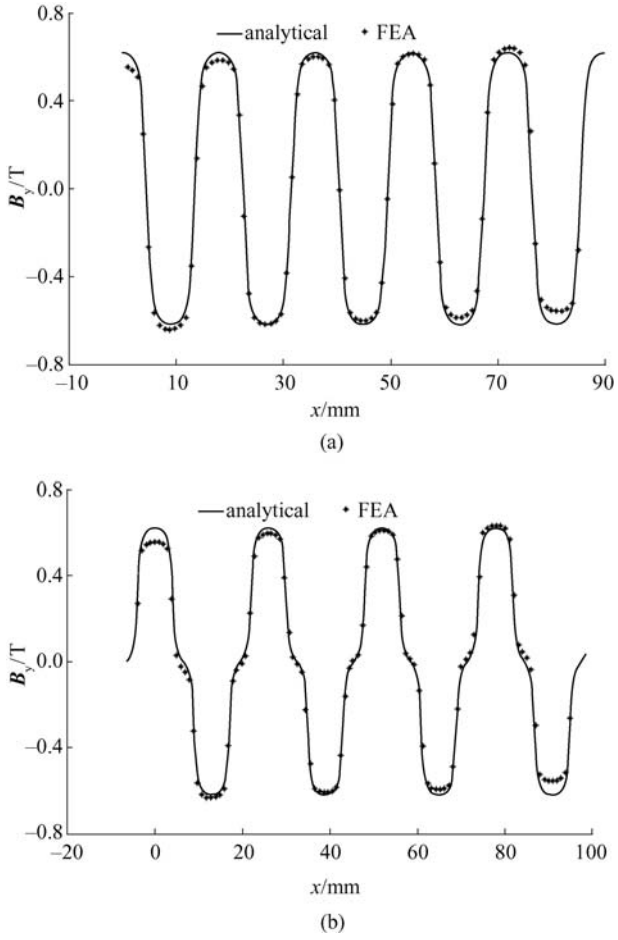

Fig. 6 Air-gap flux density distribution of conventional arrays. (a) $\varepsilon = 0.89$; (b) $\varepsilon = 0.62$

simplified, the calculation results accords with that of ANSYS. Moreover, the analysis method used in this paper can be applied in the context of an iron-backed linear motor simply by changing boundary conditions. A workbench with a single degree of freedom is realized based on preceding analysis.

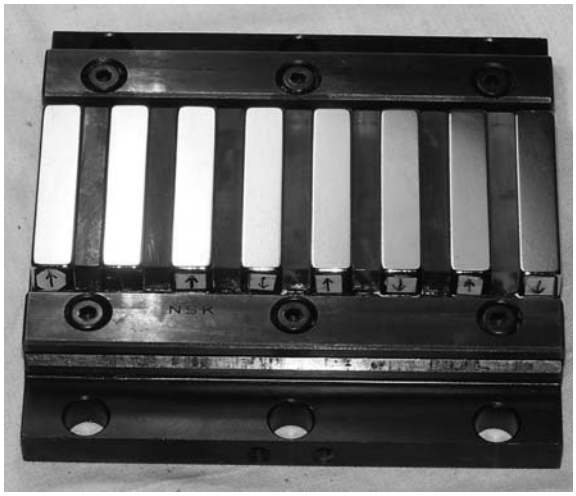

Fig. 7 Mover of linear motor

Acknowledgements This work was supported by the National Natural Science Foundation of China (Grant No. 50475083).

References

1. Guo Q D. The Precision Control Technology of Linear AC Servo System. Beijing: China Machine Press, 2000 (in Chinese)
2. Trumper D L, Williams M E, Nguyen T H. Magnet arrays for synchronous machines. Conference Record of the 1993 IEEE Industry Applications Society Annual Meeting. Piscataway: IEEE, 1993, 1: 9–18
3. Trumper D L, Kim W J, Williams M E. Design and analysis framework for linear permanent-magnet machines. IEEE Transactions on Industry Applications, 1996, 32(2): 371–379
4. Tang Y Q. Electromagnetic Field in Machine. Beijing: Science Press, 1998, 10–11 (in Chinese)
5. Halbach K. Design of permanent multipole magnets with oriented rare earth cobalt material. Nuclear Instruments and Methods, 1980, 169(1): 1–10
6. Zhang M T, Xiao R H. Electromagnetic Field of Machine. Beijing: China Machine Press, 1988, 82–85 (in Chinese)